npj | climate and atmospheric science

Article

Published in partnership with CECCR at King Abdulaziz University

https://doi.org/10.1038/s41612-025-01113-w

Accelerated shifts from heatwaves to heavy rainfall in a changing climate

Jian Li[1], Shuo Wang[1,2] ✉, Jinxin Zhu[3], Dagang Wang[3] & Tongtiegang Zhao[4]

Consecutive heatwave and heavy rainfall (HW-HR) events are occurring with increasing frequency in a warming climate. The time interval, defined as the duration between the end of a heatwave and the onset of heavy rainfall, affects both environmental conditions and the regional recovery between two consecutive extreme events. However, the dynamics of the transition between consecutive HW-HR events remain poorly understood. In this study, we examine the changes in the time interval of consecutive HW-HR events in China from 1970 to 2019, using meteorological data from over 2000 stations across mainland China. Our results reveal that the time interval has significantly shortened at 24.1% of the stations. This trend is primarily driven by an increased proportion of short-time events (STEs), defined as consecutive events with time intervals within 1–2 days. From 1970 to 2019, the proportion of STEs increased significantly, at a rate of 1.4% per decade. We also find that climate change-induced anomalies in atmospheric variables during the consecutive HW-HR events, especially convective available potential energy, 2 m temperature, and relative humidity, may contribute to this rise in the proportion of STEs. Additionally, our study assesses changes in population exposure to STEs over the past two decades. We find that the area of exposure has increased across more than three-quarters of the country, with the increases in STEs contributing to 65.3% of the overall rise in exposure. Our findings highlight the importance of prioritizing disaster response during consecutive HW-HR events and implementing effective risk management strategies to mitigate population exposure to extreme events.

Heatwaves and extreme rainfalls are the two extreme events with significant impacts on human health, food, and the environment[1–3]. The heatwaves refer to a prolonged period of much-warmer-than-average weather[4]. Prolonged heating causes the atmosphere to store energy, increasing the likelihood of extreme rainfall shortly after a heatwave ends[5]. Under climate change, the frequency of both heatwaves and extreme rainfall has increased[6–12]. During the summer of 2023, China experienced 14 extreme heat events, with about 70% of national weather stations recording temperatures above 40 °C[13]. Simultaneously, 37 extreme precipitation events occurred, with 55 stations recording unprecedented rainfall amounts[14]. High-frequency, widespread extreme weather events increase the interdependence between heatwaves and rainfall, causing regions to be consecutively affected over short periods[15–17]. For example, in July 2023, North China faced persistent heat followed by rare extreme rainfall, with cumulative precipitation reaching 1003 mm, resulting in significant losses[18]. In 2023, extreme weather events in China led to direct economic losses of 330.6 billion RMB and 537 people dead or missing[14]. The frequency and intensity of heatwaves and heavy rainfalls are projected to keep increasing through the end of the century[19–22]. Along with rapid population growth, extreme events are likely to have even stronger societal impacts in the future[23–27].

Heatwaves and heavy rainfall have been widely studied as independent extreme events. However, recent research has confirmed the theoretical possibility of their consecutive occurrence[28–33]. During heatwaves, the atmosphere can store more moisture as it heats up. This moisture condenses into cloud droplets due to cooling at the end of heatwaves[34,35]. Prolonged thermal accumulation also provides energy for the formation of heavy rainfall, especially thunderstorms and convective precipitation, and

[1]Department of Land Surveying and Geo-Informatics, The Hong Kong Polytechnic University, Hong Kong, China. [2]Research Institute for Land and Space, The Hong Kong Polytechnic University, Hong Kong, China. [3]Carbon-Water Observation and Research Station in Karst Regions of Northern Guangdong, School of Geography and Planning, Sun Yat-Sen University, Guangzhou, China. [4]State Key Laboratory of Water Resources Engineering and Management & Southern Marine Science and Engineering Guangdong Laboratory (Zhuhai), School of Civil Engineering, Sun Yat-Sen University, Guangzhou, China.
✉e-mail: shuo.s.wang@polyu.edu.hk

increases instability in the upper troposphere[36,37]. When the heatwave ends, moisture in the lower troposphere converges and lifts above the unstable upper troposphere, resulting in heavy rainfall. These studies show a strong thermodynamic link between heatwaves and heavy rainfall[28,32]. At the same time, synoptic weather systems, such as fronts and low-pressure cyclones, can also lead to a spatial and temporal consecutive occurrence between heatwaves and heavy rainfall[38–40]. These systems might even terminate a heatwave, leading to heavy rainfall shortly thereafter[41,42]. Based on the theoretical possibility of consecutive heatwave and heavy rainfall (HW-HR) events, existing studies have explored patterns and dynamics of probability, frequency, duration, intensity, and future projections, offering a comprehensive understanding of these compound events[5,15,43–46]. Additionally, previous studies have examined the mechanisms and factors influencing these events by considering the characteristics of the independent HW-HR events, climate anomalies during the compound event, and human activities[30,47–52]. Furthermore, previous studies have also explored the spatial compounding of these two events. For example, Li et al.[53] explored the connection between the heatwave in Pakistan and heavy rainfall in the middle and lower reaches of the Yangtze River as a spatially compound event, based on atmospheric circulation and tele-connection.

Compound or consecutive extreme events can have a greater social impact than single extreme events in terms of direct economic losses, energy, agricultural yields, and human health[54–56]. This is because the initial event often alters the environmental preconditions, reducing the region's ability to resist the subsequent events[31,57]. In this context, the time interval between consecutive extreme events, such as abrupt transitions between dry and wet periods, has raised concerns and proven to be particularly critical[58,59]. If the time interval is too short, the affected region may not have sufficient time to recover from the effects of the previous event, which may exacerbate the impact of following events[60,61]. For instance, during July 2021 in Western Europe, a persistent and extreme heatwave was followed by intense rainfall, causing catastrophic flooding and heat stress risks for residents[62,63]. Although the time interval between consecutive HW-HR events is critically important due to their destructive impacts and superimposed losses, few studies have focused on this aspect[49,64], as well as the changes in this interval and underlying mechanisms remain unknown. Understanding these changes as well as their societal impacts is essential for enhancing disaster warning systems, improving emergency management, and reducing climate change-related losses.

The objective of this study is to examine the changes in the time interval between consecutive HW-HR events in China from 1970 to 2019, using station observations. Additionally, we analyzed potential physical mechanisms affecting these time intervals with meteorological variables from the ERA5 reanalysis dataset. Finally, we examined changes in population exposure to consecutive HW-HR events with short time intervals over the past five decades using population data. This study provides valuable insights into compound extreme events and their societal impacts, aiding in targeted disaster response and climate change mitigation, and adaptation strategies.

Results

Characteristics and dynamics of the time interval between consecutive heatwave and heavy rainfall (HW-HR) events

Figure 1 illustrates the pattern and evolution of time intervals between consecutive HW-HR events from 1970 to 2019. The average time interval across all stations during this period is 3.32 days. Notably, 98.7% of stations have an average time interval of less than 5 days, indicating that in most consecutive HW-HR events, heavy rainfall typically occurs within 5 days after the heatwave ends (Fig. 1b). In terms of spatial distribution, there is no clear hot or cold spot. However, inland areas in Southwest China tend to have shorter time intervals. Similarly, stations in northern regions, including North and Northwest China, also exhibit shorter time intervals, generally below the national average. In contrast, Northeast and East China tend to have relatively longer time intervals (Fig. 1a and Supplementary Fig. S1). Regions with shorter intervals align with regions identified in previous studies as having a higher probability of consecutive HW-HR events[47,49]. This suggests that these areas may experience more frequent and rapid shifts from heatwaves to heavy rainfall. From 1970 to 2019, more than half of the stations show a decreasing trend in time intervals, with 22.5% of stations exhibiting a significant decrease. This suggests that at many stations, the interval between the end of a heatwave and the onset of heavy rainfall is becoming shorter. Conversely, 18.2% of the stations show a significant increasing trend (Fig. 1c, d). Since the number of stations with significant increases is roughly equal to those with significant decreases, there is no overall significant trend in the average time interval across all stations. However, in hotspot regions such as Northeast China, the time intervals show significant decreasing trends (Supplementary Fig. S2).

We further examine the most urgent type of event: the short-time events (STEs). Figure 2b shows that the STEs account for a significantly higher proportion of events than the other two types, which are middle-time events (MTEs) and long-time events (LTEs), at most stations. At 32.8% of the stations, STEs constitute more than half of all consecutive HW-HR events. Stations with a high proportion of STEs are primarily located in Southwest China, consistent with the spatial pattern of shorter average time interval (Fig. 2a). In terms of temporal changes, 24.1% of the stations show a significant increase in the proportion of STEs from 1970 to 2019 (Fig. 2c). In Northeast, East and South China, stations with significant increases in the proportion of STEs are relatively concentrated and exhibit a higher rate of change compared to other regions (Supplementary Fig. S1). The average proportion of STEs across all stations also shows a significant increasing trend ($p < 0.05$), with a rate of 1.4% per decade (Fig. 2d). There is a strong negative correlation ($R = -0.77$, $p < 0.01$) between shortened time intervals and the increased proportion of STEs. Furthermore, 79.8% of stations show a consistent relationship between the trend of the average time interval and the trend of STE proportion (blue dots in Fig. 2e). Specifically, these stations are located in the second and fourth quadrants of the scatter plot, indicating that a decrease in the time interval is generally associated with an increase in the STE proportion, and vice versa. This suggests that the rise in the proportion of STEs is a key driver of the shortening time intervals.

We also examine the consecutive HR-HW events (Supplementary Fig. S3). The proportion of STEs within HR-HW events remains relatively low. At the same time, the number of stations with a high proportion of STEs and a significantly increasing trend in STEs is also relatively low compared to the HW-HR events. The relatively low frequency of consecutive HR-HW events is consistent with previous studies[15,65]. However, the proportion of STEs within HR-HW events still shows a significant increasing trend, further supporting our point that the connection between heatwaves and heavy rainfall has intensified under the changing climate.

It is important to note that there are four possible explanations for the increase in the proportion of STEs. First, both STEs and consecutive HW-HR events may be increasing, but the frequency of STEs increases at a faster rate than the frequency of consecutive HW-HR events. Second, it is possible that while the frequency of STEs increases, the total frequency of consecutive HW-HR events remains unchanged, leading to a higher proportion of STEs. Third, STEs could increase even if the total frequency of consecutive HW-HR events decreases. In this case, the proportion of STEs rises not due to an increase in STE frequency, but because of a reduction in consecutive HW-HR events. Finally, both STEs and consecutive HW-HR events may decrease, but if STEs decline at a slower rate than total consecutive HW-HR events, the proportion of STEs would still increase. Supplementary Fig. S4 shows the frequencies of STEs, MTEs, LTEs, and all consecutive HW-HR events. Over the past five decades, all four event types have exhibited a significant increasing trend, suggesting that the increase in the proportion of STEs is primarily due to their faster rate of increase compared to all consecutive HW-HR events.

Attribution of the increasing proportion of short-time events (STEs)

Heavy rainfall events have a strong temperature dependency[66]. Under global warming, the frequency and intensity of independent HW-HR events have

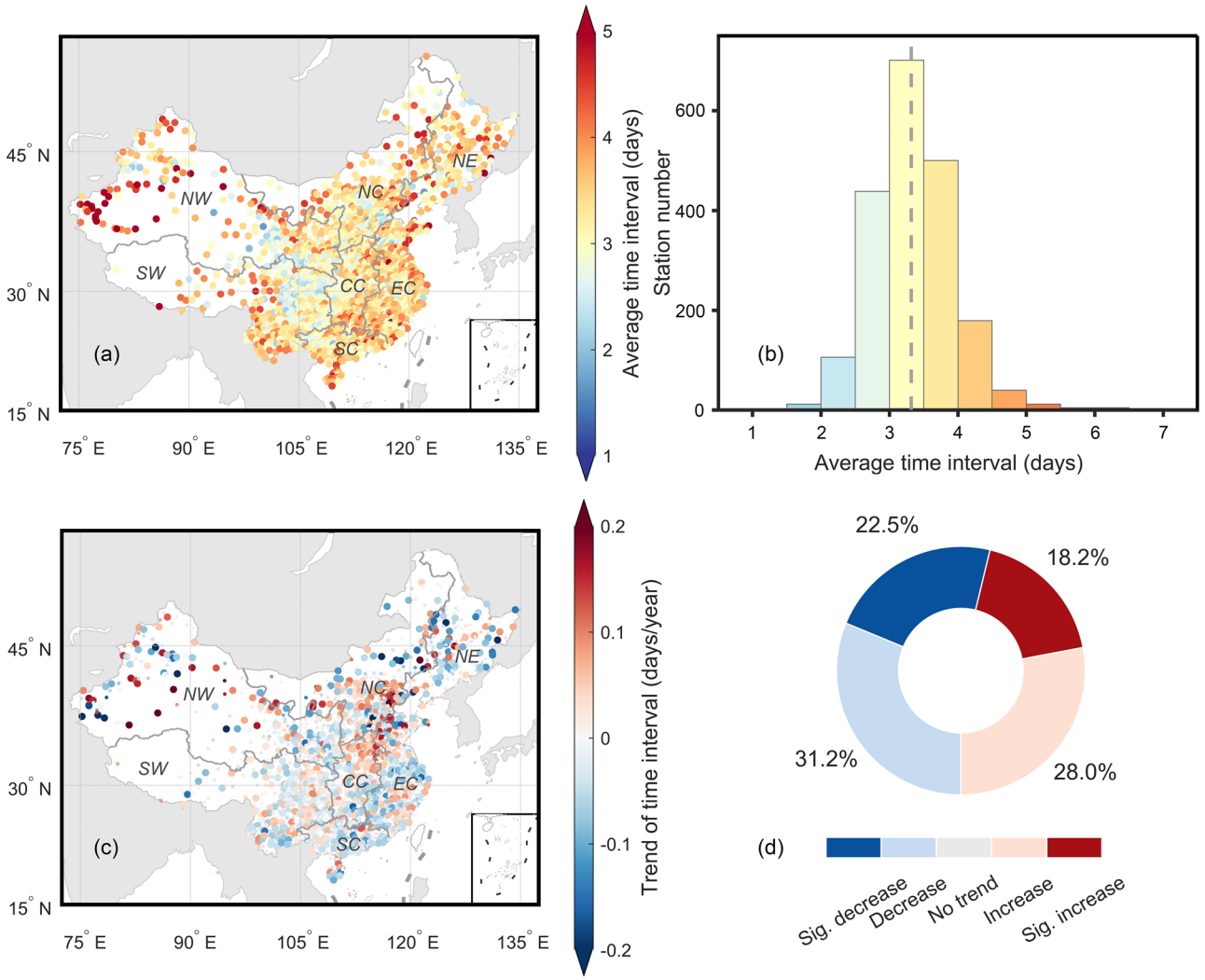

Fig. 1 | Spatial distributions and trends of average time interval. a Average time interval at each station during the study period from 1970 to 2019. **b** Statistics of station numbers based on time interval. **c** Trend of time interval of each station during the study period from 1970 to 2019. Large dots indicate trends that are significant at the 95% confidence level, while small dots represent trends that are not significant. **d** Statistics summary of station proportion based on trend significance. The abbreviations of sub-regions can be found in the section "Methods".

been shown to increase[67]. The significance test proves that the frequency of consecutive HW-HR events is significantly higher than the 95% confidence interval estimates derived from moving-blocks bootstrap resampling[65,68], which indicate that the occurrence of consecutive HW-HR events is triggered by underlying mechanisms rather than random chance (Supplementary Fig. S5). Heatwaves significantly modify atmospheric thermodynamic conditions, thereby promoting the occurrence of extreme precipitation events[49]. Elevated levels of atmospheric energy and moisture increase instability[36,47,69,70]. During heatwaves, high temperatures and reduced cloud cover result in strong thermal forcing, leading to substantial energy accumulation in the atmosphere[71–73]. As the heatwave ends, this accumulated energy is released, creating conditions more conducive to convection and even thunderstorms[32]. According to the Clausius–Clapeyron relationship, the moisture-holding capacity of the atmosphere increases by about 7% for every 1 °C rise in temperature[29,35]. Therefore, moisture from enhanced evaporation and convergence during heatwaves is retained in the atmosphere. Once the heatwave ends and temperatures decline, the stored moisture is lifted to the condensation level, triggering deep convection and intense precipitation[30,35,70], thereby enhancing the likelihood of extreme precipitation events in the period following the end of the heatwave[45,74]. All these factors may have shortened the time interval between heatwaves and heavy rains, increasing the proportion of STEs. To assess the contribution of multiple factors to the increase in the STEs proportion, we employed an XGBoost (eXtreme Gradient Boosting) classifier model combined with SHAP (SHapley Additive explanation) to investigate the impact of atmospheric variables and dominant weather types on the occurrence of STEs. (Supplementary Text S1 and Fig. S6).

Existing studies have demonstrated the impact of convective available potential energy (CAPE) anomalies on consecutive HW-HR events[69]. During heatwaves, rising temperatures lead to energy accumulation in the atmosphere, causing an increase in CAPE[75]. After the heatwave ends, CAPE generally decreases, often resulting in negative ΔCAPE values. Our study finds that a higher value of ΔCAPE also accelerates the transition from heatwaves to heavy rains. The 10-year moving average of ΔCAPE anomaly showed a significant increasing trend at most stations from 1970 to 2019 (Fig. 3a). The yearly average of ΔCAPE also indicates a significant increasing trend over the past five decades, with STEs exhibiting notably higher ΔCAPE values than LTEs (Fig. 3b). The larger ΔCAPE in STEs suggests that CAPE remains relatively high even after the heatwave ends, leading to a more unstable atmosphere and increasing the likelihood of heavy rainfall occurring within a short interval[76]. Similarly, the spatial pattern of 2 m temperature (T2M) anomalies change in Fig. 3c shows a significant increase in T2M anomalies during the interval periods. T2M anomalies exhibited a notable upward trend, with STEs having significantly higher T2M

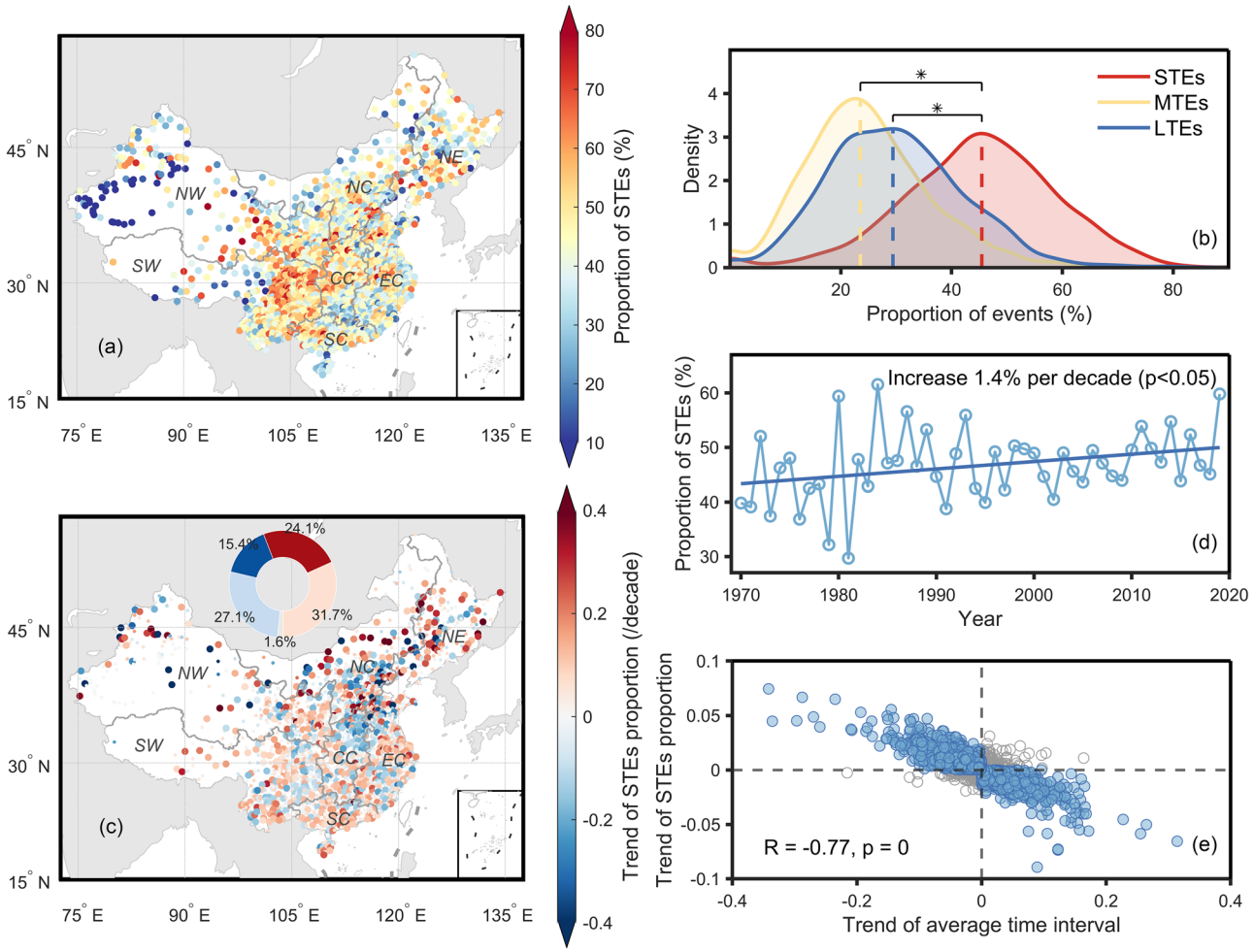

Fig. 2 | Spatial distributions and trends of short-time events (STEs) proportion. **a** Proportion of STEs at each station during the study period from 1970 to 2019. **b** Density plot of station distributions by the proportion of STEs, medium-time events (MTEs), and long-time events (LTEs). The density is estimated using kernel density estimation with a Gaussian kernel function and a bandwidth of 1000 for each event type. The colored dashed lines corresponding to each event type indicate the median proportion of each type. The asterisk (*) denotes significant differences between the STEs and MTEs/LTEs, calculated using Student's *t*-test at the 95% confidence level. **c** Trend of STEs proportion per decade for each station during the study period from 1970 to 2019. Large dots indicate trends that are significant at the 95% confidence level, while small dots represent trends that are not significant. The inset provides a statistical summary of station proportions based on trend significance, where dark red represents a significant increase, while dark blue indicates a significant decrease. **d** Trend of average STEs proportion across all stations. The dotted line represents annual values, and the solid line represents the linear trend. **e** Correlation between the trend of STEs proportion and the average time interval. Blue dots represent stations where the two variables exhibit opposite trends. Correlation analysis is based on the Pearson correlation test. The abbreviations of sub-regions can be found in the section "Methods".

anomalies than LTEs (Fig. 3d). Higher T2M anomalies in STEs indicate that even after the heatwave ends, the atmosphere retains a high temperature and stored energy, which enhances atmospheric instability and provides favorable conditions for heavy rainfall formation[77]. These findings suggest that under the changing climate, atmospheric energy accumulation after heatwaves has been increasing, leading to greater atmospheric instability during the interval in STEs compared to LTEs.

Besides energy and heat, the atmospheric moisture conditions also play a crucial role in the development of heavy rainfall. Changes in relative humidity (RH) and evaporation (ET) anomalies reflect these moisture conditions (Fig. 3e–h). High temperatures during a heatwave remove a large amount of soil moisture. After the heatwave ends, less soil moisture is available for evaporation. As the duration and magnitude of heatwaves increased, both STEs and LTEs experienced a significant decline in ET anomalies during the interval period[78]. However, RH anomalies during the interval do not exhibit a significant trend (Fig. 3f). Notably, RH anomalies in STEs intervals are significantly higher than in LTEs intervals, indicating that despite reduced soil evaporation, the atmosphere retains substantial moisture during STEs intervals, which provide conditions for heavy rainfall formation[79]. This may be due to the higher ET during the STEs intervals compared to LTEs, which contributes additional moisture to the atmosphere (Fig. 3h). Moreover, convective conditions may further enhance atmospheric moisture content through moisture convergence[80], as the average moisture convergence on the horizontal level during STEs intervals shows a significantly increasing trend (Supplementary Fig. S7). Spatially, in the hotspots where the STEs proportion has increased significantly, such as South China, the RH and ET anomalies even show a pattern of localized aggregated increase (Fig. 3e, g). This suggests that in STEs-prone regions, more moisture is retained in the atmosphere after a heatwave, maintaining evaporation intensity and providing moisture for extreme precipitation within short intervals.

Assessment of population exposure to short-time events (STEs)

The increasing proportion of STEs raises risks to human health and society. On one hand, people are exposed to rapid shifts in temperature and humidity, which can predispose them to neurological and psychiatric diseases[81,82]. On the other hand, heatwaves often coincide with droughts, leading to increased water repellency in soil and reduced infiltration[27,83,84].

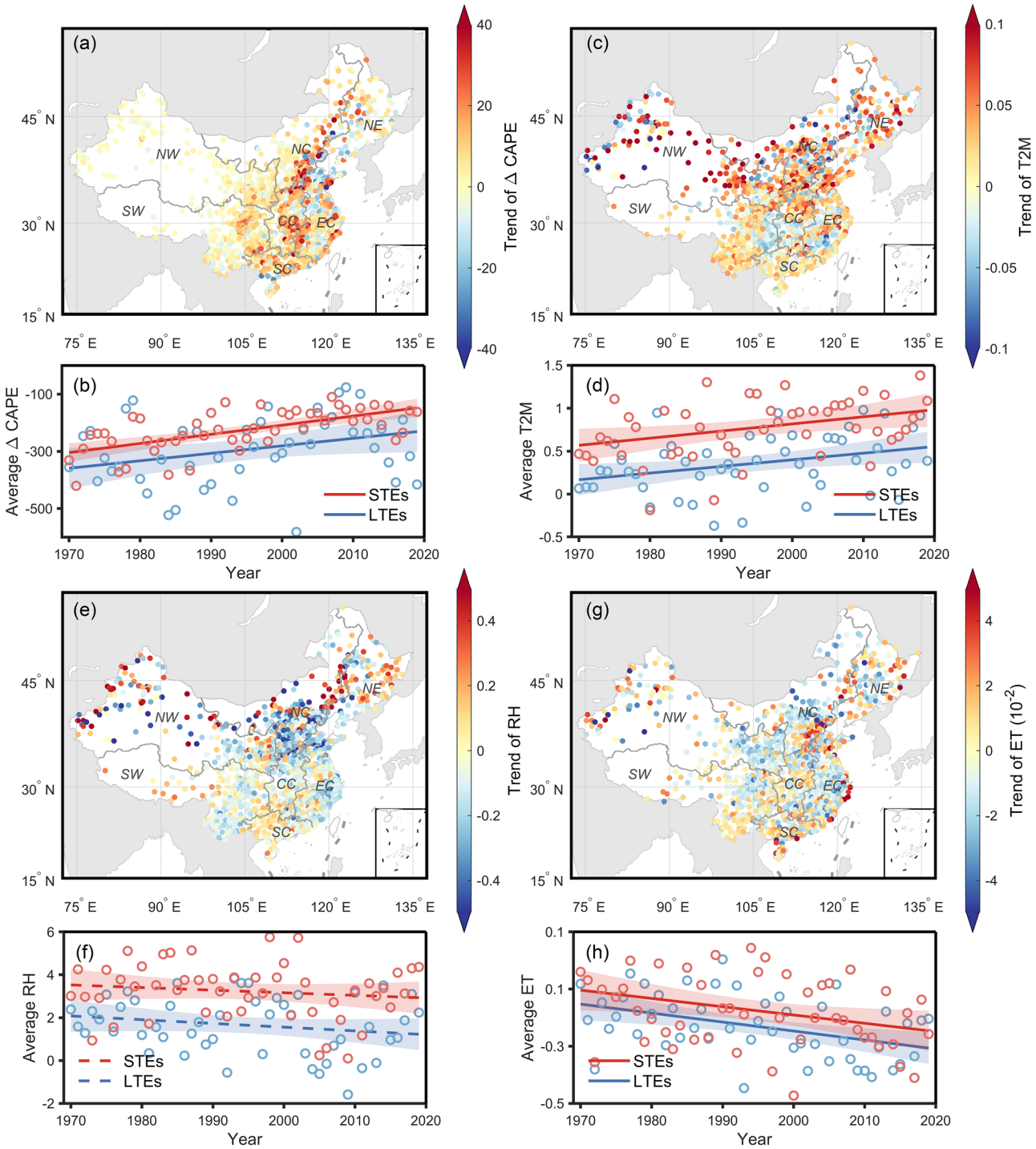

Fig. 3 | Trend patterns and yearly trend of anomalies for four atmospheric variables. The panels **a**, **c**, **e**, **g** show the trend patterns and the panels **b**, **d**, **f**, **h** show the yearly trends. **a**, **b** Convective Available Potential Energy (CAPE, J/kg), representing the change of CAPE between interval average and the end of heatwave, **c**, **d** 2 m temperature (T2M, °C), **e**, **f** Relative Humidity (RH, %), and **g**, **h** Evaporation (ET, mm) during consecutive heatwave and heavy rainfall events. Only stations with significant changes at the 95% confidence level are shown in the trend patterns. The abbreviations of sub-regions can be found in the section "Methods".

Extreme precipitation following a heatwave can trigger flooding, and the shortened interval between extreme events presents a greater challenge to society's ability to respond to floods[85].

In the past five decades, the population exposed to STEs in China has increased more than fivefold, rising from 87.7 million persons · events in 1975 to 585.5 million persons · events in 2020. The exposure proportion also surged from 9.5% to 40.8% (Fig. 4c). A total of 84.7% of stations show an increasing trend, covering 75.7% of the entire country's area (Fig. 4b). The stations with rising exposure are widely distributed, with the highest rates of change observed in the South (852.9%) and East China (478.0%) (Supplementary Fig. S8). Notably, eight urban agglomerations have experienced above-average increases in exposure (Fig. 4d), including the Yangtze River Delta (YRD) and Pearl River Delta (PRD), China's two largest urban agglomerations, where both population and STE frequency have risen sharply.

Increased exposure to extreme weather events can be influenced by both climate and population factors[86]. To assess their respective contributions, we further examine the effects of population growth and the rise in

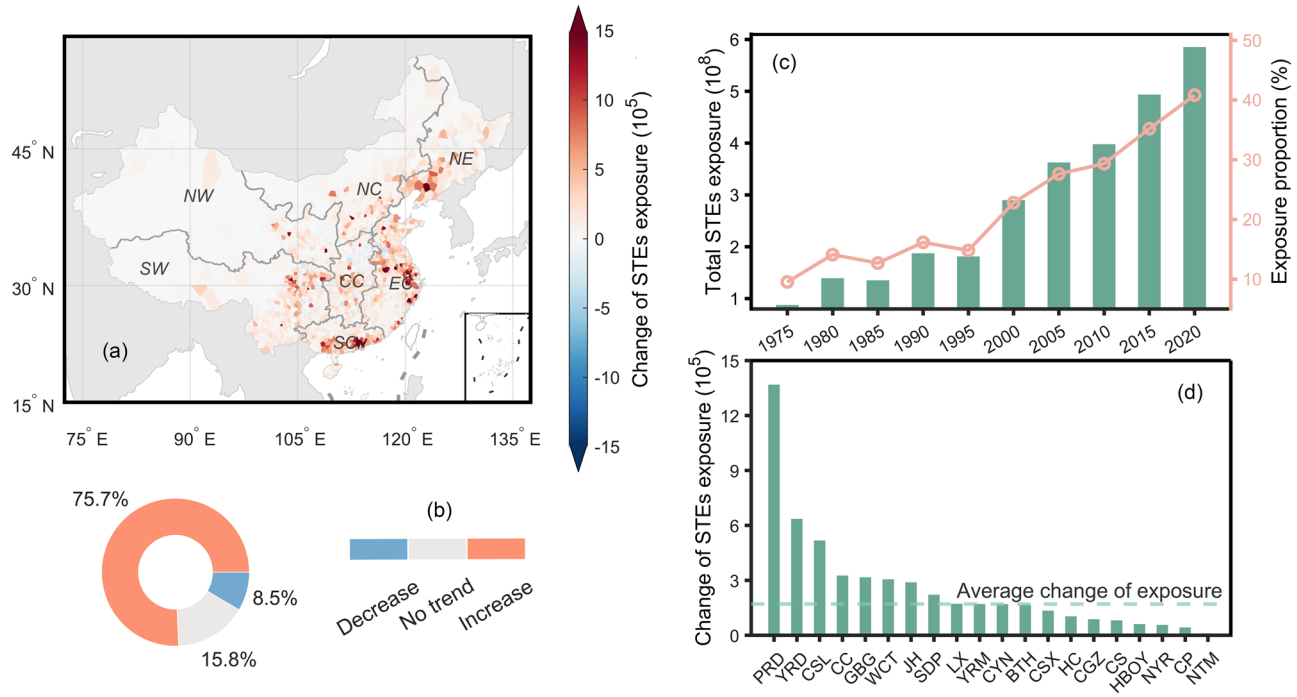

Fig. 4 | Dynamics of short-time events (STEs) exposure from 1975 to 2020. **a** Spatial pattern of changes in STEs exposure. **b** Area proportion of STEs exposure changes. **c** Dynamics of total population exposed to STEs (bars) and proportion of population exposed to STEs (dotted line), and **d** Changes in STEs exposure in the 20 major urban agglomerations of China (see Supplementary Table S1 for details). The abbreviations of sub-regions can be found in the section "Methods".

STEs (Supplementary Text S2 and Fig. S9). The results indicate that the increase in STEs is the dominant factor, contributing 65.3% to the rise in exposure. Despite rapid population growth over the past five decades, its direct contribution remains relatively low (8.2%) due to the rarity of STEs in the early years of the study period. However, the interaction between population growth and climate change plays a significant role, contributing 26.5% to the overall increase. In the agglomerations experiencing both rapid population growth and intensified climate change, such as PRD and YRD, the interaction effects can be particularly high, reaching 66.1% and 44.7%, respectively.

Discussion

While the characteristics of consecutive HW-HR events have been extensively studied, less attention has been given to the dynamic evolution of time intervals between these consecutive events in a changing climate. This study focuses on the changes in the time interval between consecutive HW-HR events in China over a 30-year period, using meteorological observations. By integrating meteorological variables and socio-economic data, we reveal the changing characteristics, underlying mechanisms, and social impacts of the changing time interval between consecutive HW-HR events under climate change. Understanding these changes is crucial for mitigating social risks associated with compounded extreme events.

Our study found that 24.1% of the stations in China exhibited a significant decreasing trend in the average time interval between consecutive HW-HR events from 1970 to 2019. The increase in the proportion of STEs (1–2 days) is an important reason for the shortening of the average time intervals. The proportion of STEs increased significantly at a rate of 1.4% per decade on a national scale, with hotspots increasing at rates of 5.3% per decade in Northeast China, 3.1% per decade in South China, and 2.2% per decade in East China. Shifts in anomalies of atmospheric variables lead to changes in energy and moisture during consecutive HW-HR events, thereby contributing to the increased proportion of STEs. Compared to LTEs, STEs experienced a significant increase in CAPE and T2M, as well as higher positive anomalies in RH and ET, presenting conditions that were more conducive to the formation of extreme precipitation at the end of the heatwave. With urbanization and increased population, the exposure to STEs in China has increased by more than fivefold over the past five decades, with more than three-quarters of the areas showing an increase in exposure. The rising frequency of STEs was mainly responsible for this increase in exposure, with a contribution rate of 65.3%.

Thresholds used to identify extreme events can affect their characteristics. To ensure the robustness of our results, we examined outcomes using different definitions. Heatwave thresholds were set at the 85th, 90th, and 95th percentiles, while heavy rainfall thresholds were at the 90th, 95th, and 99th percentiles. Supplementary Fig. S10 shows the results of sensitivity experiments. Although there were variations in the number of events detected, the conclusions of our study remained consistent. We define consecutive events as those with a total time interval of less than 7 days between a HW-HR, and STEs as the consecutive events with time intervals of 1–2 days. This classification may also introduce some uncertainty. Therefore, we tested different combinations of total time intervals and STEs thresholds to further assess sensitivity (Supplementary Fig. S11). Under various combinations of STEs thresholds and total time intervals, most of the proportion of STEs showed a significant increasing trend. The sensitive experiments indicate that the time interval between consecutive HW-HR events is shortening in a changing climate.

Considering only consecutive HW-HR events occurring at the same station is the ideal scenario. In reality, consecutive HW-HR events may occur at larger spatial domains[87]. Our study provides a preliminary exploration of spatially consecutive HW-HR events (Supplementary Text 3 and Fig. S12). We observed that within a 1° spatial buffer, the frequency of spatially consecutive HW-HR events is significantly lower than the frequency of consecutive HW-HR events occurring at the same station. Moreover, spatially consecutive events did not exhibit distinct hotspot areas, which demonstrated the significance of our study even without considering spatially consecutive HW-HR events. However, the characteristics of spatially consecutive HW-HR events deserve further exploration, as they are influenced by atmospheric motions that could display notable trends under climate change.

The shortening of the time interval between consecutive HW-HR events may result from the interaction between multiple factors. Previous

studies have proved that urbanization may cause impacts on extreme events by altering local microclimates and land surface properties[88–91]. Atmospheric circulation and synoptic weather systems can also intensify the linkage between the HW-HR. Additionally, topography also has significant effects on the formation of convective precipitation[70,92]. To better separate the impact of each factor on the time interval, it is essential to use multiple sources of data, such as high-resolution satellite remote sensing data for precipitation and temperature, as applied in studies of independent HW-HR events[50,93,94]. In addition, heatwaves may influence atmospheric chemical compositions and processes, potentially accelerating subsequent heavy rainfall. During heatwaves, atmospheric aerosol concentrations and properties change, possibly affecting atmospheric moisture and energy transport processes[95–97]. However, the microscopic mechanisms by which aerosols influence consecutive HW-HR events and their time intervals are currently unclear. Future studies could explore the interactive feedback between meteorological variables and aerosols using regional chemistry transport models such as WRF-Chem.

Our study focuses on the dynamic evolution of the time intervals between consecutive HW-HR events and their social implications. The results have practical implications for climate change policy and urban development planning. On one hand, we observe an enhanced dependence between temperature extremes and heavy rainfall events, along with a shortening of the interval, which highlights the urgent need for policymakers to address the conditions under which heavy rainfall occurs shortly after a heatwave. This necessitates enhancing early warning systems, improving public awareness, and facilitating timely evacuation plans to minimize casualties and property damage. On the other hand, our study reveals that the combined effects of climate change and urbanization are increasing population exposure to consecutive events in large urban agglomerations, such as the YRD and PRD. This implies that more urbanized areas are facing greater risks from extreme events. To address these risks, urban planning should integrate climate change adaptation strategies, such as developing resilient infrastructure and improving drainage systems. Furthermore, rationalizing the spatial distribution of urban populations can help reduce exposure to natural disasters. Policies such as decentralizing urban centers, promoting sustainable urbanization, and encouraging the development of smaller cities can alleviate the pressure on megacities. By aligning urban development policies with climate risks, the resilience of urban agglomerations to extreme events can be significantly enhanced.

Methods

Data

The daily maximum temperature data and daily precipitation data are obtained from the Resource and Environmental Science Data Platform (https://www.resdc.cn/), covering the period from 1970 to 2019. This dataset has been widely used in climate change studies across mainland China[29,98]. The daily records have been processed by the China National Meteorological Information Center of the China Meteorological Administration to ensure quality and homogeneity[99]. The original dataset includes a total of 2474 stations. To maintain completeness and continuity in the historical records, we apply selection criteria based on WMO standard practices[100]. First, stations with missing data for 3 consecutive years are excluded. Second, a month is considered unavailable if there are more than 11 missing values in total or if there are 5 consecutive missing values. Stations with more than 5 unavailable months during the study period are also excluded. After applying these criteria, 2001 stations are retained for the study.

The atmospheric variables used for attribution are derived from the European Centre for Medium-Range Weather Forecasts Reanalysis 5 (ERA5) hourly data on single levels (https://cds.climate.copernicus.eu/datasets/reanalysis-era5-single-levels?tab=download). The spatial resolution is 0.25° × 0.25°, and we select the nearest grid point to each station to represent the local climate conditions. The time resolution has been aggregated from hourly to a daily scale.

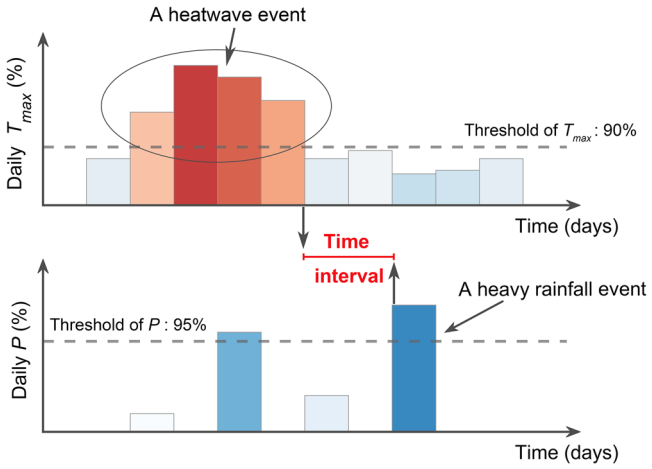

Fig. 5 | Schematic for identifying the time interval between consecutive heatwaves and heavy rainfall events. Each bar represents a one-day period. T_{max} and P represent the maximum temperature and precipitation, respectively. Concurrent events (shown as the first blue bar above the threshold line) are not considered in this research.

The population data used for exposure calculations are obtained from the Global Human Settlement Layer dataset[101]. The spatial resolution of the data is 30 × 30 arcseconds (~900 m near the equator) and covers the period from 1975 to 2020 at 5-year intervals.

The administrative boundary data was obtained from the National Geomatics Center of China (http://www.ngcc.cn/ngcc/). The study area was divided into seven sub-regions based on geographical location and socio-economic conditions: Northeast China (NE), North China (NC), Northwest China (NW), East China (EC), Central China (CC), Southwest China (SW), and South China (SC). The boundaries of these sub-regions, along with station locations and population information, are presented in Supplementary Fig. S13.

Identification and characterization of the time interval between consecutive heatwave and heavy rainfall (HW-HR) events

As depicted in Fig. 5, consecutive HW-HR events refer to the consecutive occurrence of HW-HR events. Heatwave is identified when the daily maximum temperature exceeds a threshold (the 90th percentile in this study) for at least 3 consecutive days during the extended summer season (May to September). To minimize the impact of station location and seasonality, the threshold is calculated for each station and each calendar day[29,102]. Specifically, for each station, we select the 7 days before and after each calendar day (a 15-day window) within the reference period (1970–1989). This results in 300 daily maximum temperature samples (15 days × 20 years). The 90th percentile of these 300 samples is then used as the threshold for that station and calendar day. A heatwave is considered to end when the daily maximum temperature falls below the threshold for 2 consecutive days, in order to exclude the influence of data recording biases[103]. Heavy rainfall is defined as that where daily precipitation exceeds the 95th percentile of the baseline period and occurs within 7 days after the end of a heatwave. If the total time interval between HW-HR exceeds 7 days, the events are treated as independent[64]. In this study, we focus on the time interval between the end of a heatwave and the first occurrence of heavy rainfall (Fig. 5). Concurrent HW-HR events are not considered in this study.

After identifying all consecutive HW-HR events, we categorize them into three groups based on their time intervals. Specifically, events with an interval of 1 or 2 days are classified as STEs, events with 3 or 4 days are classified as MTEs, and events with an interval of 5–7 days are classified as LTEs. By comparing the meteorological variable anomalies across the different event types, we identify significantly higher energy and moisture levels in STEs (Fig. S14). These findings support the physical mechanism for categorizing and analyzing different types of consecutive HW-HR events.

Sensitivity tests regarding the definition of these three types of events are provided in the Discussion and Supplementary Information. The time interval for each station is calculated for each 5-year time window. Trend analysis is performed using linear regression, and the significance of the trend values is tested using the Mann–Kendall test.

Attribution of the shortened time intervals

The accelerated transition from heatwave to heavy rainfall may be influenced by various atmospheric variables. To identify the most influential factors, we apply the XGBoost (eXtreme Gradient Boosting) classifier model[104] combined with SHAP (SHapley Additive explanation) to rank the contribution of relevant factors (see Supplementary Text S1). Based on the results of the XGBoost model, we select four atmospheric variables: CAPE, T2M, RH, and ET. We use the yearly trend to analyze the anomaly changes during the interval of STEs and LTEs, therefore, to compare the potential contributions of these variables to trigger the more frequent STEs. The yearly trend is calculated by the Mann–Kendall test.

We also conduct regional analysis to ensure whether the most influential atmospheric variables are consistent across different regions in China. The results in Fig. S15 show that, although there are slight variations in the ranking of contributing factors across different regions, ΔCAPE, RH anomalies, and T2M anomalies consistently play dominant roles.

Calculation of the exposure to the short-time events (STEs)

We use the number of people exposed to extreme events to examine the evolution of exposure from 1975 to 2020 for every 5 years (i.e., 1975, 1980, 1985, 1990, 1995, 2000, 2005, 2010, 2015, and 2020), based on the availability of population data. Accordingly, for each available year, STEs frequency is calculated as the average of 2 years prior to and the 2 years following the target year. The number of people exposed to extreme events is determined based on the risk assessment framework[105] and is defined as Eq. (1):

$$Exposure = \sum_{i=1}^{n} POP_i \times STEF_i \quad (1)$$

where $STEF_i$ represents the frequency of STEs in station i. POP_i represents the number of people within the areas affected by station i. The affected area for each station is defined by the Thiessen polygon method, which is commonly used to extend the observation data to ranges[99]. After building the Thiessen polygons, we apply the zonal statistics methods to aggregate the population data from grid cells to polygons.

Data availability

The daily maximum temperature and daily precipitation data are obtained from the Resource and Environmental Science Data Platform (https://www.resdc.cn/). The atmospheric variables are obtained from the European Centre for Medium-Range Weather Forecasts Reanalysis 5 (ERA5) hourly data on single levels (https://cds.climate.copernicus.eu/datasets/reanalysis-era5-single-levels?tab=download). Population data are obtained from the Global Human Settlement Layer (GHSL) dataset (https://human-settlement.emergency.copernicus.eu/).

Code availability

All relevant codes are available from the corresponding author upon reasonable request.

Received: 3 January 2025; Accepted: 3 June 2025;
Published online: 10 June 2025

References

1. Garcia-Leon, D. et al. Current and projected regional economic impacts of heatwaves in Europe. *Nat. Commun.* **12**, 5807 (2021).
2. Mora, C. et al. Broad threat to humanity from cumulative climate hazards intensified by greenhouse gas emissions. *Nat. Clim. Change* **8**, 1062–1071 (2018).
3. Ridder, N. N. et al. Global hotspots for the occurrence of compound events. *Nat. Commun.* **11**, 5956 (2020).
4. IPCC. Annex VII: Glossary. *Climate Change 2021: The Physical Science Basis* (Cambridge University Press, 2021).
5. Sauter, C. et al. Compound extreme hourly rainfall preconditioned by heatwaves most likely in the mid-latitudes. *Weather Clim. Extrem.* **40**, 100563 (2023).
6. Cai, W. et al. Increased frequency of extreme Indian Ocean Dipole events due to greenhouse warming. *Nature* **520**, 254–259 (2014).
7. Christidis, N. et al. Dramatically increasing chance of extremely hot summers since the 2003 European heatwave. *Nat. Clim. Change* **5**, 46–50 (2014).
8. Perkins-Kirkpatrick, S. E. et al. Increasing trends in regional heatwaves. *Nat. Commun.* **11**, 3357 (2020).
9. Barriopedro, D. et al. Heat waves: physical understanding and scientific challenges. *Rev. Geophys.* **61**, e2022RG000780 (2023).
10. Sun, Q. et al. A global, continental, and regional analysis of changes in extreme precipitation. *J. Clim.* **34**, 243–258 (2021).
11. Hartmann, D. L. et al. Changes in the distribution of rain frequency and intensity in response to global warming. *J. Clim.* **27**, 8372–8383 (2014).
12. Cai, F. et al. Sketching the spatial disparities in heatwave trends by changing atmospheric teleconnections in the Northern Hemisphere. *Nat. Commun.* **15**, 8012 (2024).
13. WMO. *State of the Climate in Asia 2023* (World Meteorological Organization, 2024).
14. CMA. *China Climate Bulletin 2023* (China Meteorological Administration, 2023).
15. Miao, L. et al. Unveiling the dynamics of sequential extreme precipitation-heatwave compounds in China. *npj Clim. Atmos. Sci.* **7**, 67 (2024).
16. Zhou, P. et al. Likelihood of concurrent climate extremes and variations over China. *Environ. Res. Lett.* **13**, 094023 (2018).
17. Zscheischler, J. et al. Dependence of drivers affects risks associated with compound events. *Sci. Adv.* **3**, e1700263 (2017).
18. Sun, L. et al. State of China's climate in 2023. *Atmos. Ocean. Sci. Lett.* **17**, 100519 (2024).
19. Fischer, E. M. et al. Anthropogenic contribution to global occurrence of heavy-precipitation and high-temperature extremes. *Nat. Clim. Change* **5**, 560–564 (2015).
20. Meehl, G. A. et al. More intense, more frequent, and longer lasting heat waves in the 21st Century. *Science* **305**, 994–997 (2004).
21. Chen, D. et al. Contribution of anthropogenic influence to the 2022-like Yangtze River valley compound heatwave and drought event. *npj Clim. Atmos. Sci.* **7**, 172 (2024).
22. Christidis, N. et al. Rapidly increasing likelihood of exceeding 50 °C in parts of the Mediterranean and the Middle East due to human influence. *npj Clim. Atmos. Sci.* **6**, 45 (2023).
23. Wu, S. et al. Urbanization-driven increases in summertime compound heat extremes across China. *Sci. Total Environ.* **799**, 149166 (2021).
24. Newman, R. et al. The global costs of extreme weather that are attributable to climate change. *Nat. Commun.* **14**, 6103 (2023).
25. Ghanbari, M. et al. The role of climate change and urban development on compound dry-hot extremes across US cities. *Nat. Commun.* **14**, 3509 (2023).
26. Yin, J. et al. Future socio-ecosystem productivity threatened by compound drought–heatwave events. *Nat. Sustain.* **6**, 259–272 (2023).
27. Tripathy, K. P. et al. Climate change will accelerate the high-end risk of compound drought and heatwave events. *Proc. Natl. Acad. Sci. USA* **120**, e2219825120 (2023).
28. Cloutier-Bisbee, S. R. et al. Heat waves in Florida: climatology, trends, and related precipitation events. *J. Appl. Meteorol. Climatol.* **58**, 447–466 (2019).

29. Lenderink, G. et al. Super-Clausius–Clapeyron scaling of extreme hourly convective precipitation and its relation to large-scale atmospheric conditions. *J. Clim.* **30**, 6037–6052 (2017).
30. Li, C. et al. Urbanization-induced increases in heavy precipitation are magnified by moist heatwaves in an urban agglomeration of east China. *J. Clim.* **36**, 693–709 (2023).
31. Wang, S. S. Y. et al. Consecutive extreme flooding and heat wave in Japan: Are they becoming a norm? *Atmos. Sci. Lett.* **20**, e933 (2019).
32. Sauter, C. et al. Compounding heatwave-extreme rainfall events driven by fronts, high moisture, and atmospheric instability. *J. Geophys. Res. Atmos.* **128**, e2023JD038761 (2023).
33. Raghavendra, A. et al. Floridian heatwaves and extreme precipitation: future climate projections. *Clim. Dyn.* **52**, 495–508 (2018).
34. White, R. H. et al. The unprecedented Pacific Northwest heatwave of June 2021. *Nat. Commun.* **14**, 727 (2023).
35. Trenberth, K. E. et al. The changing character of precipitation. *Bull. Am. Meteorol. Soc.* **84**, 1205–1217 (2003).
36. Zhang, Y. et al. An upper bound for extreme temperatures over midlatitude land. *Proc. Natl. Acad. Sci. USA* **120**, e2215278120 (2023).
37. Wang, S. Y. et al. Identification of extreme precipitation threat across midlatitude regions based on short-wave circulations. *J. Geophys. Res. Atmos*. **118**, 11-059 (2013).
38. Boschat, G. et al. Large scale and sub-regional connections in the lead up to summer heat wave and extreme rainfall events in eastern Australia. *Clim. Dyn.* **44**, 7–8 (2014).
39. Yu, Y. et al. Characteristics analysis and synoptic features of event-based regional heatwaves over China. *J. Geophys. Res. Atmos.* **126**, e2020JD033865 (2021).
40. Pfahl, S. Characterising the relationship between weather extremes in Europe and synoptic circulation features. *Nat. Hazards Earth Syst. Sci.* **14**, 1461–1475 (2014).
41. Choi, W. et al. Synoptic conditions controlling the seasonal onset and days of heatwaves over Korea. *Clim. Dyn.* **57**, 3045–3053 (2021).
42. Tencer, B. et al. Compound temperature and precipitation extreme events in southern South America: associated atmospheric circulation, and simulations by a multi-RCM ensemble. *Clim. Res.* **68**, 183–199 (2016).
43. Zhou, Z. et al. Global increase in future compound heat stress-heavy precipitation hazards and associated socio-ecosystem risks. *npj Clim. Atmos. Sci.* **7**, 33 (2024).
44. Sauter, C. et al. Temporally compounding heatwave–heavy rainfall events in Australia. *Int. J. Climatol.* **43**, 1050–1061 (2022).
45. Ren, J. et al. Downscaled compound heatwave and heavy-precipitation analyses for Guangdong, China in the twenty-first century. *Clim. Dyn.* **61**, 2885–2905 (2023).
46. Ning, G. et al. Rising risks of compound extreme heat-precipitation events in China. *Int. J. Climatol.* **42**, 5785–5795 (2022).
47. You, J. et al. Higher probability of occurrence of hotter and shorter heat waves followed by heavy rainfall. *Geophys. Res. Lett.* **48**, e2021GL094831 (2021).
48. Vicedo-Cabrera, A. M. et al. The burden of heat-related mortality attributable to recent human-induced climate change. *Nat. Clim. Change* **11**, 492–500 (2021).
49. Sun, P. et al. Are longer and more intense heatwaves more prone to extreme precipitation? *Glob. Planet. Change* **236**, 104428 (2024).
50. Wu, S. et al. Increasing compound heat and precipitation extremes elevated by urbanization in South China. *Glob. Planet. Change* **9**, 636777 (2021).
51. Chen, B. et al. The evolution of social-ecological system interactions and their impact on the urban thermal environment. *npj Urban Sustain* **4**, 3 (2024).
52. Olmo, M. et al. Atmospheric circulation influence on temperature and precipitation individual and compound daily extreme events: Spatial variability and trends over southern South America. *Weather Clim. Extrem.* **29**, 100267 (2020).
53. Li, S. et al. East Asian summer rainfall stimulated by subseasonal Indian monsoonal heating. *Nat. Commun.* **14**, 5932 (2023).
54. Zscheischler, J. et al. Future climate risk from compound events. *Nat. Clim. Change* **8**, 469–477 (2018).
55. Raymond, C. et al. Understanding and managing connected extreme events. *Nat. Clim. Change* **10**, 611–621 (2020).
56. Leonard, M. et al. A compound event framework for understanding extreme impacts. *WIREs Clim. Change* **5**, 113–128 (2013).
57. Deng, S. et al. Global distribution and projected variations of compound drought-extreme precipitation events. *Earth's Future* **12**, e2024EF004809 (2024).
58. Chen, H. et al. Accelerated transition between dry and wet periods in a warming climate. *Geophys. Res. Lett.* **49**, e2022GL099766 (2022).
59. Chen, Y. et al. Detectable increases in sequential flood-heatwave events across china during 1961–2018. *Geophys. Res. Lett.* **48**, e2021GL092549 (2021).
60. Zscheischler, J. et al. A typology of compound weather and climate events. *Nat. Rev. Earth Environ.* **1**, 333–347 (2020).
61. Chen, Y. et al. Greater flash flood risks from hourly precipitation extremes preconditioned by heatwaves in the Yangtze River Valley. *Geophys. Res. Lett.* **49**, e2022GL099485 (2022).
62. Tradowsky, J. S. et al. Attribution of the heavy rainfall events leading to severe flooding in Western Europe during July 2021. *Clim. Change* **176**, 90 (2023).
63. Lhotka, O. et al. The 2021 European heat wave in the context of past major heat waves. *Earth Space Sci.* **9**, e2022EA002567 (2022).
64. Zhang, J. et al. A new method to identify the maximum time interval between individual events in compound rainstorm and heatwave events. *Int. J. Disaster Risk Sci.* **15**, 453–466 (2024).
65. You, J. et al. Growing threats from swings between hot and wet extremes in a warmer world. *Geophys. Res. Lett.* **50**, e2023GL104075 (2023).
66. Barbero, R. et al. Temperature-extreme precipitation scaling: a two-way causality? *Int. J. Climatol.* **38**, e1274–e1279 (2018).
67. Qian, C. et al. Human influences on spatially compounding flooding and heatwave events in China and future increasing risks. *Weather Clim. Extrem.* **42**, 100616 (2023).
68. Vogel, R. M. et al. The moving blocks bootstrap versus parametric time series models. *Water Resour. Res.* **32**, 1875–1882 (1996).
69. Zhang, W. et al. Deadly compound heat stress-flooding hazard across the Central United States. *Geophys. Res. Lett.* **47**, e2020GL089185 (2020).
70. Liu, J. et al. Understanding compound extreme precipitations preconditioned by heatwaves over China under climate change. *Environ. Res. Lett.* **19**, 064077 (2024).
71. Randall, D. A. et al. Intercomparison and interpretation of surface energy fluxes in atmospheric general circulation models. *J. Geophys. Res. Atmos.* **97**, 3711–3724 (1992).
72. Zhang, T. et al. An energetics tale of the 2022 mega-heatwave over central-eastern China. *npj Clim. Atmos. Sci.* **6**, 162 (2023).
73. Tian, Y. et al. Characterizing heatwaves based on land surface energy budget. *Commun. Earth Environ.* **5**, 617 (2024).
74. Li, W. et al. Anthropogenic impact on the severity of compound extreme high temperature and drought/rainevents in China. *npj Clim. Atmos. Sci* **6**, 79 (2023).
75. Meyer, J. et al. Atmospheric conditions favouring extreme precipitation and flash floods in temperate regions of Europe. *Hydrol. Earth Syst. Sci.* **26**, 6163–6183 (2022).
76. Chen, J. et al. Changes in convective available potential energy and convective inhibition under global warming. *J. Clim.* **33**, 2025–2050 (2020).
77. Berg, P. et al. Strong increase in convective precipitation in response to higher temperatures. *Nat. Geosci.* **6**, 181–185 (2013).

78. Zhou, T. J. et al. Atmospheric water vapor transport associated with typical anomalous summer rainfall patterns in China. *J. Geophys. Res. Atmos.* **110**, D08104 (2005).
79. Ou, Q. et al. Relating extreme precipitation events to atmospheric conditions and driving variables in China. *Clim. Dyn.* **62**, 4925–4942 (2024).
80. Yang, L. et al. Sensitivity of extreme rainfall to atmospheric moisture content in the arid/semiarid southwestern United States: implications for probable maximum precipitation estimates. *J. Geophys. Res. Atmos.* **123**, 1638–1656 (2018).
81. Ban, J. et al. Projecting future excess deaths associated with extreme precipitation events in China under changing climate: an integrated modelling study. *Lancet Planet. Health* **8**, e723–e733 (2024).
82. Sisodiya, S. M. et al. Climate change and disorders of the nervous system. *Lancet Neurol.* **23**, 636–648 (2024).
83. Mukherjee, S. et al. Increase in compound drought and heatwaves in a warming world. *Geophys. Res. Lett.* **48**, e2020GL090617 (2021).
84. Gimbel, K. F. et al. Does drought alter hydrological functions in forest soils? *Hydrol. Earth Syst. Sci.* **20**, 1301–1317 (2016).
85. Matanó, A. et al. Compound and consecutive drought-flood events at a global scale. *Environ. Res. Lett.* **19**, 064048 (2024).
86. Manoli, G. et al. Magnitude of urban heat islands largely explained by climate and population. *Nature* **573**, 55–60 (2019).
87. Li, M. et al. The linkage of the large-scale circulation pattern to a long-lived heatwave over mideastern China in 2018. *Atmosphere* **10**, 89 (2019).
88. Salvi, K. A. et al. Imprint of urbanization on snow precipitation over the continental USA. *Nat. Commun.* **15**, 2348 (2024).
89. Schug, F. et al. The global wildland-urban interface. *Nature* **621**, 94–99 (2023).
90. Zhou, Y. et al. Satellite mapping of urban built-up heights reveals extreme infrastructure gaps and inequalities in the Global South. *Proc. Natl. Acad. Sci. USA* **119**, e2214813119 (2022).
91. Liao, W. et al. Stronger contributions of urbanization to heat wave trends in wet climates. *Geophys. Res. Lett.* **45**, 310–317 (2018).
92. Zhou, L. et al. Vertical structures of abrupt heavy rainfall events over southwest China with complex topography detected by dual-frequency precipitation radar of Global Precipitation Measurement satellite. *Int. J. Climatol.* **42**, 7628–7647 (2022).
93. Sethi, S. S. et al. Urbanization and regional climate change-linked warming of Indian cities. *Nat. Cities* **1**, 402–405 (2024).
94. Peng, J. et al. Diversified evolutionary patterns of surface urban heat island in new expansion areas of 31 Chinese cities. *npj Urban Sustain.* **4**, 14 (2024).
95. Leung, G. R. et al. Aerosol breezes drive cloud and precipitation increases. *Nat. Commun.* **14**, 2508 (2023).
96. Wang, P. et al. Aerosols overtake greenhouse gases causing a warmer climate and more weather extremes toward carbon neutrality. *Nat. Commun.* **14**, 7257 (2023).
97. Stier, P. et al. Multifaceted aerosol effects on precipitation. *Nat. Geosci.* **17**, 719–732 (2024).
98. Lin, X. et al. Urbanization amplified compound hot extremes over the three major urban agglomerations in China. *Geophys. Res. Lett.* **51**, e2023GL106644 (2024).
99. Yang, Y. et al. Variations in summertime compound heat extremes and their connections to urbanization in China during 1980–2020. *Environ. Res. Lett.* **17**, 064024 (2022).
100. WMO. *WMO Guidelines on the Calculation of Climate Normals* (World Meteorological Organization, 2017).
101. Schiavina, M. et al. GHS-POP R2023A—GHS population grid multitemporal (1975-2030). (European Commission, Joint Research Centre (JRC), 2023).
102. Gao, S. et al. Urbanization-induced warming amplifies population exposure to compound heatwaves but narrows exposure inequality between global North and South cities. *npj Clim. Atmos. Sci.* **7**, 154 (2024).
103. Perkins, S. E. et al. On the measurement of heat waves. *J. Clim.* **26**, 4500–4517 (2013).
104. Chen, T. & Guestrin, C. XGBoost: a scalable tree boosting system. In *Proc. 22nd ACM SIGKDD International Conference on Knowledge Discovery and Data Mining* 785–794. https://doi.org/10.1145/2939672.2939785 (Association for Computing Machinery, 2016).
105. Fang, P. et al. Substantial increases in compound climate extremes and associated socio-economic exposure across China under future climate change. *npj Clim. Atmos. Sci.* **8**, 17 (2025).

Acknowledgements

This research was supported by the National Natural Science Foundation of China (Grant No. 42301021) and the Hong Kong Polytechnic University (Grant No. P0052737).

Author contributions

S.W. and J.L. designed the study. J.L. carried out the analysis and drafted the manuscript. S.W. supervised the analysis and contributed to the interpretation and discussion of the results. J.Z., D.W., and T.Z. collected and pre-processed the observational data. All authors revised and edited the manuscript.

Competing interests

The authors declare no competing interests.

Additional information

Supplementary information The online version contains supplementary material available at https://doi.org/10.1038/s41612-025-01113-w.

Correspondence and requests for materials should be addressed to Shuo Wang.